Measuring evolution of a photon in an interferometer with spectrally resolved modes

Marek Bula,[1] Karol Bartkiewicz,[2,1] Antonín Černoch,[1] Dalibor Javůrek,[1] Karel Lemr,[1,*] Václav Michálek,[3] and Jan Soubusta[3]

[1]*RCPTM, Joint Laboratory of Optics of Palacký University and Institute of Physics of Czech Academy of Sciences, 17. listopadu 12, 771 46 Olomouc, Czech Republic*

[2]*Faculty of Physics, Adam Mickiewicz University, PL-61-614 Poznań, Poland*

[3]*Institute of Physics of Czech Academy of Sciences, Joint Laboratory of Optics of PU and IP AS CR, 17. listopadu 50A, 772 07 Olomouc, Czech Republic*

(Received 5 August 2016; published 9 November 2016)

In the year 2013, Danan *et al.* published a paper [Phys. Rev. Lett. **111**, 240402 (2013)] demonstrating a counterintuitive behavior of photons in nested Mach–Zehnder interferometers. The authors then proposed an explanation based on the two-state vector formalism. This experiment and the authors' explanation raised a vivid debate within the scientific community. In this paper, we contribute to the ongoing debate by presenting an alternative experimental implementation of the Danan *et al.* scheme. We show that no counterintuitive behavior is observed when performing direct spectrally resolved detection.

DOI: 10.1103/PhysRevA.94.052106

I. INTRODUCTION

Over the past three years, Vaidman and co-workers published several papers discussing a new method for analyzing the past of a photon detected at the output of an interferometer [1–5]. This method, based on the two-state vector formalism (TSVF), raised a vivid debate within the scientific community. In their seminal paper on this topic [4], Danan *et al.* presented experimental evidence for the validity of this approach. In that experiment, two nested Mach–Zehnder interferometers were constructed with mirrors A, B, C, E, and F vibrating at distinct frequencies (see Fig. 1). Harmonic analysis of the output signal allowed them to determine whether a photon passed by a specific mirror. Three different configurations were tested in the original experiment. In one of these configurations (labeled "c" in the original paper) a highly counterintuitive outcome was obtained. This result was observed when the outer interferometer was disabled by blocking its lower arm (path "c") and thus only the inner interferometer was operational. Phase shift in this inner interferometer was adjusted so that the two indistinguishable photon paths interfered destructively in the monitored output port ($\varphi = 0$).

Quite surprisingly, even the photons, whose paths in the interferometer had been identified by the harmonic analysis, interfered destructively. This effect seemingly violates the Englert–Greenberger–Yasin duality relation, which is related with the wave-particle duality of photons [6–11]. The authors of Ref. [4] claimed that "the experimental results have a simple explanation in the framework of the two-state vector formalism of quantum theory" and "even Maxwell's equations for the classical electromagnetic field should explain the observed phenomena." This particular experiment and the unusual interpretation of the results were subsequently followed by a number of papers [12–20]. Authors of these papers, for instance, provided an alternative classical formalism [12,13] for the experiment or questioned its specific implementation [14,15].

In 2015, we theoretically analyzed the Danan *et al.* experiment [4] and proposed a standard quantum-mechanical description of the action of vibrating mirrors introducing distinguishable modes [15]. In that paper, we also argued that the method used to process detected light in the Danan *et al.* experiment is not suitable because it neglects part of the signal. This is then incorrectly interpreted as observing destructive interference. In Ref. [15], we proposed a different measurement technique to reveal the path of the photon inside the interferometer. The suggested detection method is based on a direct spectral power density measurement. We predicted identical results in all configurations of the Danan *et al.* experiment except for the counterintuitive case with blocked path "c". Our detection method predicts quite intuitive results even in this configuration.

In this paper, we report on an experimental implementation of our measurement method. Instead of the vibrating mirrors we use two different frequency filters to shape spectra of the photons propagating in the upper and lower arm of the interferometer. Thus, we "leave a mark" on them which can then be used to extract which-path information during the detection stage. Our detection method and the one presented in the original paper by Danan *et al.* give incompatible results only when path "c" is blocked (see Fig. 1). In this case, the outer interferometer does not influence the results and therefore we can test our detection method by using only one Mach–Zehnder interferometer playing the same role as the inner interferometer in the Danan *et al.* experiment. Our experimental setup is sketched in Fig. 2.

Our experimental setup in described in Sec. II. In Sec. III, we describe the spectrum measurement performed and the procedure to reconstruct the photons' which-path information in a way analogous to that of the Danan *et al.* experiment [4]. In the original work [4], temporal evolution of the overall intensity was recorded and postprocessed. From the postprocessed data, the intensity spectrum was computed. In contrast to that, we measure the intensity spectrum directly and demonstrate that it is in agreement with our theoretical model presented in Ref. [15]. Additionally, we show that the obtained measurements fulfill the Englert–Greenberger–Yasin inequality [6,10]. Moreover, in Sec. IV, we use a postprocessing method similar to the one used in the original experiment [4]. Based on this approach, we explain the

*Corresponding author: k.lemr@upol.cz

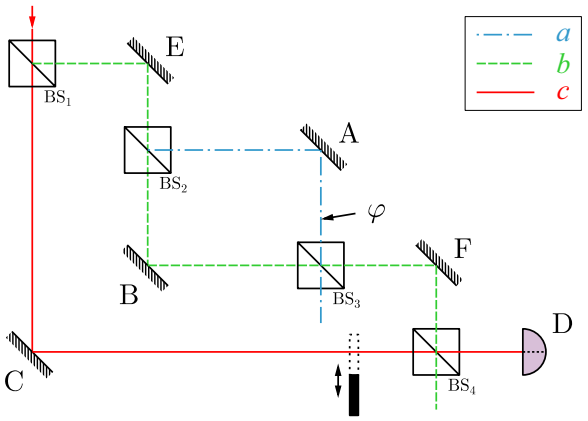

FIG. 1. Scheme of the original Danan *et al.* experiment [4]. Mirrors vibrating at various frequencies are denoted A, B, C, E, and F (upper-case letters) while the corresponding spatial modes are labeled a, b, and c (lower-case letters). Output signal is monitored on detector D. The counterintuitive result was observed when the lower arm of the outer interferometer (path "c") was blocked and the inner interferometer was set so that destructive interference occurs in the monitored output port. Even the photons known to travel by one specific arm of the inner interferometer (either mirror A or B) interfered destructively.

apparent loss of the signal that can be incorrectly attributed to destructive interference.

II. EXPERIMENTAL SETUP

Our experimental setup is based on a Mach–Zehnder interferometer as depicted in Fig. 2. The interferometer consists of two polarization independent beam splitters BS_1 and BS_2 and two pentaprisms. The input light beam is generated by a mode-locked femtosecond laser Mira (Coherent) with a central wavelength of 826 nm, 10 nm bandwidth, and the typical mean power of 1 W. The light is coupled into the interferometer through the beam splitter BS_1. The motorized translation stage in the lower arm is used to balance the lengths of both interferometer arms. The piezo translation stage in the upper arm is used to change the relative phase between these arms. In this experiment, we used two identical narrow-band spectral filters F_1 and F_2 with transmission bandwidth of 3 nm centered at 826 nm. F_2 was mounted on a rotation stage. By rotating the filter, we were able to shift its transmission window to shorter wavelengths. In our experiment, filters F_1 and F_2 introduce distinguishability between the interferometer arms just as the vibrating mirrors did in the original paper [4]. Finally, the beam splitter BS_2 couples the light from both the interferometer arms. Due to technological imperfections, BS_1 and BS_2 have not perfectly balanced splitting ratios. Also, the overall transmissivity of F_2 depends on its rotation. Therefore, a neutral-density filter (NDF) was inserted into the upper arm to balance effective losses. The monochromator (MC) Jobin Yvon Triax 320 is located in one of the interferometer output ports and provides the capability to discriminate spectral components of the beam (shown in Fig. 2). Light was transferred from the output port of BS_2 to this monochromator by using a single-mode fiber to maximize spatial mode indistinguishability. Detection was performed at the output of the monochromator by using a power meter PM120 by Thorlabs (labeled D).

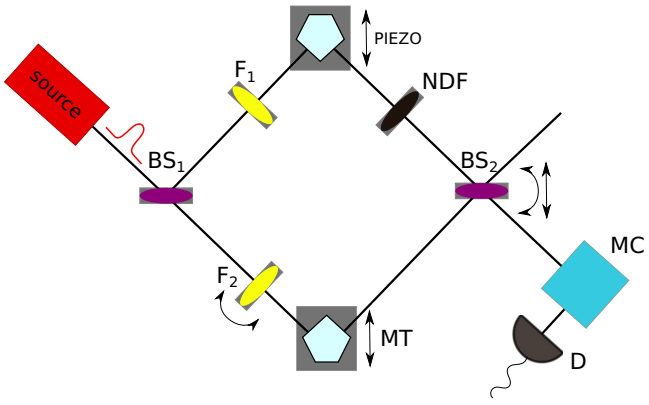

FIG. 2. Experimental setup as described in the text. Individual components are labeled as follows: BS_1 and BS_2 are beam splitters, NDF is a neutral-density filter, F_1 and F_2 are narrow-band filters, MT is a motor translation, MC is a monochromator, and D is a detector. Note that, instead of using vibrating mirrors, we encode the which-path information by shaping the light spectrum by using filters F_1 and F_2.

For the preliminary adjustments of the setup, both filters F_1 and F_2 were rotated perpendicular to the light beam direction and the detector was placed directly to the BS_2 output port bypassing thus the monochromator. First, we ensured precise coupling of the beam to the setup. We checked that the polarization remains unchanged while being transmitted or reflected on beam splitters. The second part of the adjustment procedure consists of several steps, which have to be repeated for each setting of the measurement. Balanced output intensities from both arms are achieved by rotating the NDF wheel with gradient absorption. Then the lengths of the arms were equalized by positioning the translation stage MT. Accurate setting of the MT position was adjusted by finding the maximum of the autocorrelation function of the signal. We were able to reach visibility of the interferometer typically about 98% in the initial configuration with filter F_2 inserted perpendicularly to the beam. The interferometer was sufficiently stable to scan the interference fringes by varying voltage on the piezo-driven translation stage.

III. MEASUREMENT AND RESULTS

The purpose of our experiment is to recreate a similar situation as in the original research paper by Danan *et al.* [4]. But instead of using vibrating mirrors, we encode the which-path information directly into different shapes of spectra in the upper and lower interferometer arm. Further to that, our experimental configuration allows us to tune the distinguishability between the interferometer arms. This is achieved by rotation of the second filter F_2. In subsequent paragraphs, we label three spectral modes A, B, and E in accordance with the labeling of mirrors by Danan *et al.* [4]. In the original experiment drawn in Fig. 1, mirrors A and B were placed in the upper and lower arm of the interferometer, respectively. Mirror E stood in front of that

interferometer. By observing vibration frequencies, A and B thus gave information about the propagation of light in the upper and lower arm, respectively. Frequency peak E did not provide any which-path information. Similarly to that, we associate spectral modes A and B with the modes maximizing the predictability of photons propagating in the upper (mode A) and lower (mode B) arm. Mode E was chosen to give the least amount of predictability. In the original experiment [4], the modes with a Gaussian spectral profile reflected from mirrors A and B are probabilistically distinguishable by detection of their transverse spatial modes. The beams are indistinguishable if the mirrors are deviated by an equal angle from the plane of the interferometer. Therefore, except for particular times, the beams reflected from mirrors A and B are probabilistically distinguishable. In our experiment, the same is true for beams with quasi-Gaussian spectra shaped by filters F_1 and F_2. The probabilistic distinguishability in transversal spatial modes is interchanged with probabilistic distinguishability in spectrum.

We have performed several sets of measurements for assorted rotation angles of F_2. Each measurement set consists of several scans through the frequency spectrum in the range from 815 to 835 nm with a resolution of 0.2 nm. First, we simply measured spectra separately from the upper and lower arm. We used these data to calculate theoretical predictions for the visibility. Next, for each wavelength we measured the visibility of interference as a measure of indistinguishability between the arms. The visibility is calculated from the minimal $I_{\min}$ and maximal $I_{\max}$ power density in an interference fringe at a given wavelength λ by using the formula

$$V(\lambda) = \frac{I_{\max}(\lambda) - I_{\min}(\lambda)}{I_{\max}(\lambda) + I_{\min}(\lambda)}. \quad (1)$$

The uncertainty of the power density measurement was estimated from the typical fluctuation of the power measurement of the power meter D. A typical example of one set of these spectrum scans is depicted in Fig. 3 including interference fringes at three selected wavelengths.

Based on this spectrum scan, we selected three wavelengths corresponding to the maximum and two minima of visibility. These wavelengths are labeled E for maximum of the visibility and A, and B for the two minima. Both arms contribute by equal power density at the wavelength E, thus we observe maximal interference visibility at this wavelength for the given

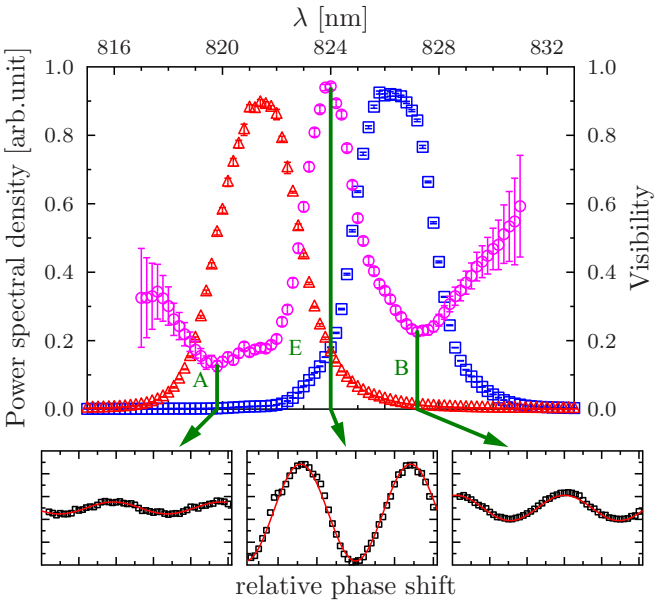

FIG. 3. Example of measured data for F_2 rotated by 14° resulting in $\Delta\lambda = 4.9$ nm. Triangles and squares represent independent spectral power density for lower and upper arms. Circles visualize obtained visibility. Vertical lines labeled A, E, and B mark the selected wavelengths corresponding to maximum and two minima of the visibility. Interference fringes (spectral power density as a function of mutual phase shift between interferometer arms) are visualized for the selected modes A, B, and E.

rotation of filter F_2. On the other hand, frequencies A and B are chosen to maximize the distinguishability of the two respective photon paths in the interferometer.

Four representative results of the normalized power densities are summarized in Table I and visualized in Fig. 4. Black bars depict power density maxima $I_{\max}$ corresponding to constructive interference, and gray bars depict power density minima $I_{\min}$ corresponding to destructive interference. To obtain normalized values of $I_{\max}$ and $I_{\min}$, we divided the measured spectral power densities by four times the spectral power density measured separately with one arm blocked. The factor 4 arises from the fact that only one quarter of the signal entering the interferometer leaves by the monitored

TABLE I. Measured minimum and maximum normalized power densities in an interference fringe for various rotations of the filter F_2. Theoretical prediction shown below is based on individual spectra taken from the interferometer arms separately.

		Frequency mode A		Frequency mode B		Frequency mode E	
$\Delta\lambda$		$I_{\max}$	$I_{\min}$	$I_{\max}$	$I_{\min}$	$I_{\max}$	$I_{\min}$
1.4 nm	Experiment	0.519 ± 0.005	0.089 ± 0.002	0.555 ± 0.007	0.094 ± 0.003	0.902 ± 0.006	0.014 ± 0.001
	Theory	0.525	0.076	0.542	0.067	0.945	0.001
2.4 nm	Experiment	0.388 ± 0.006	0.171 ± 0.004	0.398 ± 0.005	0.140 ± 0.003	0.868 ± 0.006	0.020 ± 0.001
	Theory	0.360	0.160	0.414	0.127	0.894	0.003
4.9 nm	Experiment	0.309 ± 0.007	0.240 ± 0.006	0.318 ± 0.005	0.199 ± 0.003	0.958 ± 0.020	0.028 ± 0.005
	Theory	0.284	0.218	0.312	0.195	0.962	0.0004
6.5 nm	Experiment	0.274 ± 0.005	0.234 ± 0.005	0.300 ± 0.006	0.214 ± 0.005	0.925 ± 0.030	0.039 ± 0.010
	Theory	0.274	0.219	0.303	0.202	0.987	0.00004

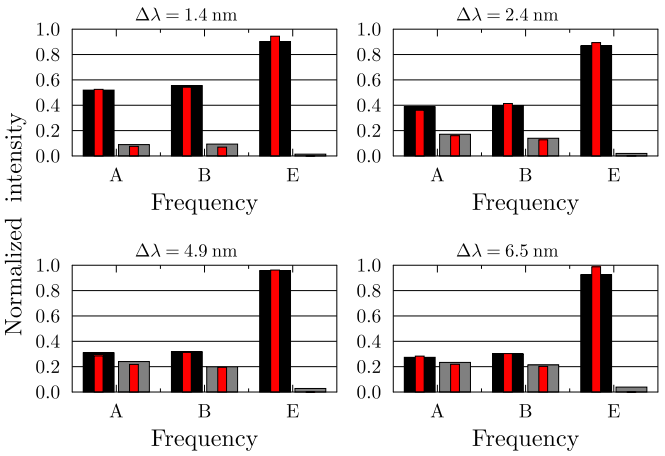

FIG. 4. Processed measurement data for four rotations of F_2, which correspond to spectral distance $\Delta\lambda = 1.4, 2.4, 4.9$, and 6.5 nm. Black bars represent normalized maximum spectral power densities (constructive interference) for wavelengths A, B, and E. Gray bars, in a similar way, represent spectral power density minima (destructive interference). Theoretical predictions are shown by using the inner red bars.

output port if one arm is blocked. As it is evident from the experimental setup shown in Fig. 2, the signal is divided in half on each of the two balanced beam splitters. Inner red bars depict theoretical predictions calculated by using the formulas for perfect constructive and destructive interference

$$I_{\max} = (\sqrt{I_1} + \sqrt{I_2})^2, \qquad I_{\min} = (\sqrt{I_1} - \sqrt{I_2})^2, \tag{2}$$

where I_1 and I_2 stand for normalized spectral power densities measured with the other interferometer arm blocked. Experimental data are in good agreement with these theoretical predictions.

As a next step, we subjected the obtained data to the Englert–Greenberger–Yasin inequality test [6,10] expressed in the form of

$$V^2(\lambda) + D^2(\lambda) \leqslant 1, \tag{3}$$

where $V(\lambda)$ stands for visibility and $D(\lambda)$ for distinguishability of the paths given by absolute value of the difference between normalized power densities from the first (I_1) and from the second arm (I_2):

$$D(\lambda) = \left| \frac{I_1(\lambda) - I_2(\lambda)}{I_1(\lambda) + I_2(\lambda)} \right|. \tag{4}$$

By using this test, we can verify the consistency of our measurements with standard quantum-mechanical limits. Our results are summarized in Table II. Note that, in the case of the original experiment by Danan *et al.*, the inequality (3) is seemingly violated, because the frequency modes A and B allegedly interfere with high visibility despite the fact that they provide exact which-path information ($D \to 1$).

Our obtained results show that, quite intuitively, the visibility decreases as the frequency modes A and B become more distinguishable (higher rotation angles of filter F_2). For perfectly distinguishable modes, visibility should drop to zero. As a result, the signal at wavelengths corresponding to frequency modes A and B is nearly constant independent of the setting of the mutual phase shift between the interferometer arms.

We observe almost perfect distinguishability when rotating the filter F_2 to achieve spectral distance $\Delta\lambda = 6.5$ nm (more then twice full width at half maximum of the relevant peaks). In this case, the situation is analogous to the experiment by Danan *et al.* with the outer interferometer blocked (see Fig. 1). Even when setting destructive interference to occur in the monitored output port, the probability of observing photons at frequencies either A or B is nonzero [see gray bars in Fig. 4 ($\Delta\lambda = 6.5$ nm)]. On the other hand, the probability of observing photons with frequency E vanishes. Measured probabilities of observing photons at frequencies A, B, and E are reaching values 0.234 ± 0.005, 0.214 ± 0.005, and 0.039 ± 0.010, respectively. Our theoretical model predicts the values to be 0.25, 0.25, and 0, respectively [15]. We attribute these small discrepancies to nonperfect distinguishability of the two modes A and B and imperfect interference at frequency E.

IV. HARMONIC ANALYSIS METHOD

Let us now focus on the differences and similarities between our experiment and the measurements performed by Danan *et al.* in Ref. [4]. They used vibrating mirrors to deflect the beam, which left a weak mark on its direction. This weak deviation was then inspected by using a quad-cell detector to measure the difference between photocurrents generated in the both halves of the detector. In our experiment, we used tunable spectral narrow-band filters to leave a which-path mark on the propagating photons instead.

For every selected wavelength, we measured an interference fringe. The maximal and minimal power intensities [$I_{\max}(\lambda)$ and $I_{\min}(\lambda)$] were used to calculate the visibility. The minima of the normalized power interference fringes are plotted in

TABLE II. Measured values of visibility V and distinguishability D for various settings of the filter F_2 rotation.

	Frequency mode A			Frequency mode B			Frequency mode E		
$\Delta\lambda$	V	D	$V^2 + D^2$	V	D	$V^2 + D^2$	V	D	$V^2 + D^2$
1.4 nm	0.71 ± 0.01	0.66 ± 0.01	0.94 ± 0.02	0.71 ± 0.01	0.64 ± 0.02	0.91 ± 0.02	0.97 ± 0.01	0.06 ± 0.01	0.94 ± 0.01
2.4 nm	0.39 ± 0.01	0.92 ± 0.02	1.00 ± 0.04	0.48 ± 0.01	0.85 ± 0.02	0.95 ± 0.03	0.95 ± 0.01	0.11 ± 0.01	0.93 ± 0.01
4.9 nm	0.13 ± 0.01	0.99 ± 0.03	1.00 ± 0.05	0.23 ± 0.01	0.97 ± 0.02	1.00 ± 0.04	0.94 ± 0.01	0.04 ± 0.01	0.89 ± 0.01
6.5 nm	0.08 ± 0.01	0.99 ± 0.02	0.99 ± 0.05	0.17 ± 0.01	0.98 ± 0.02	0.99 ± 0.05	0.92 ± 0.01	0.01 ± 0.02	0.85 ± 0.01

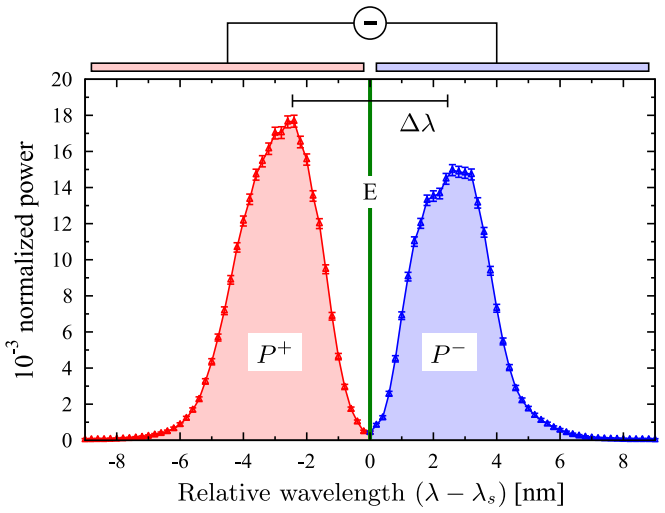

FIG. 5. Spectral dependency of normalized power of minima of interference fringe for $\Delta\lambda = 4.9$ nm. Schematically are depicted two parts of detector centered at frequency λ_s (spectral mode E). P^+ and P^- denote normalized intensities in their respective bins.

Fig. 5. The interferometer was set for destructive interference ($\varphi = 0$).

Here the monochromator is formally equivalent to the quad-cell detector distinguishing the above-mentioned marks. While the quad-cell detector registers intensity fluctuations of the resulting interference pattern due to the beam sweeping across its halves, the monochromator distinguishes the spectral marks directly. We emulate the sweep by accumulating the spectra for various rotations of filter F_2. Similar to the halves of the quad-cell detector, we divided the obtained spectra into two bins (see Fig. 5). This division between bins was made at the wavelength λ_s associated with the mode E. This mode corresponds to maximum indistinguishability like the central axis of the quad-cell detector. In Fig. 6 we summarize

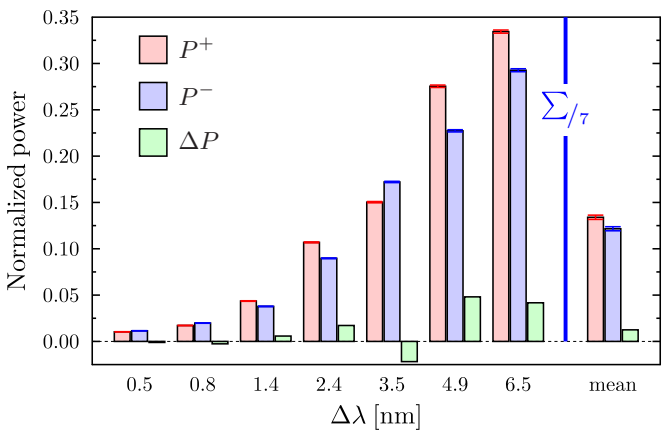

FIG. 6. The dependence of normalized powers on $\Delta\lambda$, i.e., the spectral distance between transmission maxima of filters F_1 and F_2. The last set of bars depicts the mean value corresponding to accumulation of the signal across the entire sweep.

normalized powers integrated over the two selected bins

$$P^+ = \frac{\int_0^{\lambda_s} I_{\min}(\lambda)d\lambda}{\int_0^{+\infty} I_{\max}(\lambda)d\lambda}, \quad P^- = \frac{\int_{\lambda_s}^{+\infty} I_{\min}(\lambda)d\lambda}{\int_0^{+\infty} I_{\max}(\lambda)d\lambda},$$

and their difference $\Delta P = P^+ - P^-$.

For large spectral overlap of the filters F_1 and F_2, the interference fringe is deeply modulated and the integrated minimal intensities P^+ and P^- are small. Increasing the spectral distance of the filters $\Delta\lambda$, the interference visibility decreases, leading to higher values of binned intensities P^+ and P^-. Simultaneously, the predictability of the photon path increases. But even though there is clearly a distinguishable signal from the two arms of the interferometer, ΔP simply ignores the which-path information due to the subtraction of P^+ and P^-. It does not act as a reliable which-path witness. In our experiment, the mean value of $\Delta P = 0.020 \pm 0.03$ is about one order of magnitude smaller than mean values of $P^+ = 0.134 \pm 0.002$ and $P^- = 0.122 \pm 0.002$. Ideally, ΔP should be zero. This is mathematically similar to the Danan *et al.* experiment, where they measured difference of the photocurrents generated in the two halves of the quad-cell detector. Due to the symmetry of the light profile on the detector the which-path information was lost.

V. CONCLUSIONS

In this paper, we demonstrate an alternative which-path detection method to the original harmonic analysis used in Ref. [4]. Our method is based on direct frequency resolution of the signal at the output of the interferometer. In contrast to the harmonic analysis, our method yields quite intuitive results that do not violate the Englert–Greenberger–Yasin inequality. We show that, when the frequency modes corresponding to respective arms of the interferometer are completely distinguishable, the interference vanishes and the signal is observed independently on a mutual phase shift between the interferometer arms. On the other hand, frequency modes that give no which-path information manifest high interference visibility, as expected.

We also implemented a detection method analogical to the one used in the Danan *et al.* experiment [4]. Our analysis demonstrates how the which-path information gets lost in this process. This supports our original finding [15] that, in the Danan *et al.* experiment [4], the missing signal at frequencies A and B was caused by an unsuitable detection method rather then by an interference effect. We hope that these results will further contribute to the ongoing scientific debate that follows the exciting experiment by Danan *et al.* from 2013.

ACKNOWLEDGMENTS

K.B. and K.L. acknowledge support by the Czech Science Foundation (Grant No. 16-10042Y) and the Polish National Science Centre (Grant No. DEC-2013/11/D/ST2/02638). V.M. acknowledges support by the Czech Science Foundation (Grant No. P205/12/0382). D.J. acknowledges support by the Czech Science Foundation (Grant No. 15-08971S). Finally, the authors acknowledge the Project No. LO1305 of the Ministry of Education, Youth and Sports of the Czech Republic.

[1] L. Vaidman, Impossibility of the Counterfactual Computation for All Possible Outcomes, Phys. Rev. Lett. **98**, 160403 (2007).
[2] L. Vaidman, Past of a quantum particle, Phys. Rev. A **87**, 052104 (2013).
[3] L. Vaidman, Tracing the past of a quantum particle, Phys. Rev. A **89**, 024102 (2014).
[4] A. Danan, D. Farfurnik, S. Bar-Ad, and L. Vaidman, Asking Photons Where They Have Been, Phys. Rev. Lett. **111**, 240402 (2013).
[5] L. Vaidman, "Counterfactual" quantum protocols, Int. J. Quantum Inform. **14**, 1640012 (2016).
[6] D. M. Greenberger and A. Yasin, Stimultaneous wave and particle knowledge in a neutron interferometer, Phys. Lett. A **128**, 391 (1988).
[7] M. O. Scully, B.-G. Englert, and H. Walther, Quantum optical tests of complementarity, Nature (London) **351**, 111 (1991).
[8] G. Jaeger, A. Shimony, and L. Vaidman, Two interferometric complementaries, Phys. Rev. A **51**, 54 (1995).
[9] T. J. Herzog, P. G. Kwiat, H. Weinfurter, and A. Zeilinger, Complementarity and the Quantum Eraser, Phys. Rev. Lett. **75**, 3034 (1995).
[10] B.-G. Englert, Fringe Visibility and Which-Way Information: An Inequality, Phys. Rev. Lett. **77**, 2154 (1996).
[11] P. D. D. Schwindt, P. G. Kwiat, and B.-G. Englert, Quantitative wave-particle duality and nonerasing quantum erasure, Phys. Rev. A **60**, 4285 (1999).
[12] P. L. Saldanha, Interpreting a nested Mach–Zehnder interferometer with classical optics, Phys. Rev. A **89**, 033825 (2014).
[13] V. Potoček and G. Ferenczi, Which-way information in a nested Mach–Zehnder interferometer, Phys. Rev. A **92**, 023829 (2015).
[14] H. Salih, Commentary: "Asking photons where they have been"—without telling them what to say, Front. Phys. **3**, 47 (2015).
[15] K. Bartkiewicz, A. Černoch, D. Javůrek, K. Lemr, J. Soubusta, and J. Svozilík, One-state vector formalism for the evolution of a quantum state through nested Mach-Zehnder interferometers, Phys. Rev. A **91**, 012103 (2015).
[16] Z.-Q. Wu, H. Cao, J.-H. Huang, L.-Y. Hu, X.-X. Xu, H.-L. Zhang, and S.-Y. Zhu, Tracing the trajectory of photons through Fourier spectrum, Opt. Express **23**, 10032 (2015).
[17] L. Vaidman, Comment on "One-state vector formalism for the evolution of a quantum state through nested Mach-Zehnder interferometers", Phys. Rev. A **93**, 036103 (2016).
[18] L. Vaidman, Comment on Which-way information in a nested Mach-Zehnder interferometer, Phys. Rev. A **93**, 017801 (2016).
[19] A. Danan, D. Farfurnik, S. Bar-Ad, and L. Vaidman, Response: Commentary: "Asking photons where they have been"—without telling them what to say, Front. Phys. **3**, 48 (2015).
[20] K. Bartkiewicz, A. Černoch, D. Javůrek, K. Lemr, J. Soubusta, and J. Svozilík, Reply to "Comment on 'One-state vector formalism for the evolution of a quantum state through nested Mach-Zehnder interferometers,' " Phys. Rev. A **93**, 036104 (2016).